Supporting Information

Electrocatalysis on Edge-Rich Spiral WS_2 for Hydrogen Evolution

*Prasad V. Sarma, Arijit Kayal, Chithra H. Sharma, Madhu Thalakulam, J. Mitra and M. M. Shaijumon**

School of Physics, Indian Institute of Science Education and Research Thiruvananthapuram, Maruthamala PO, Thiruvananthapuram, Kerala, 695551, India

KEYWORDS: *transition metal dichalcogenide, tungsten disulfide spirals, micro-electrocatalytic cell, conductive afm, hydrogen evolution reaction*

Email: shaiju@iisertvm.ac.in

CONTENTS

7. **Figure S6:** Mechanically exfoliated WS_2 flake: (A) Topography (B) Current map taken at dc bias +1.2V (C) Height profile (D) IV characteristics.
8. **Figure S7:** Comparing c-AFM vertical I-V response from WS_2 spiral, monolayer and mechanically exfoliated domains.
9. **Section 2: μ-electrochemical device fabrication using lithography**
10. **Figure S8**: (A) Schematic illustrating various steps involved in μ-electrochemical device fabrication
11. **Figure S9**: Optical images of WS_2 domain during different lithography steps.
12. **Figure S10:** Various devices fabricated in current study. (A) Spiral domain (B) mechanically exfoliated WS_2 and (C) Monolayer domain.
13. **Figure S11:** Polarization plot after potential correction to RHE and quasi-reference electrode potential correction.
14. **Figure S12:** Raman spectra before and after HER measurements.
15. **Table S1:** Various TMD single domain HER measurements comparison.
16. **Figure S13:** Various microelectro catalytic devices tested and polarization plots.

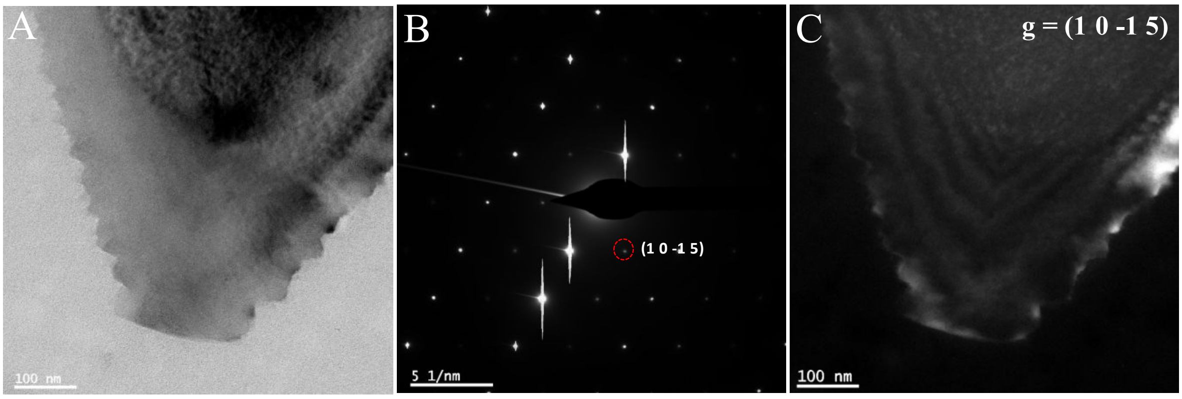

Figure S1: (A) Bright field image of a spiral edge. (B) SAED image taken from the domain edge (C) Dark field TEM image obtained from diffraction point marked in Figure B.

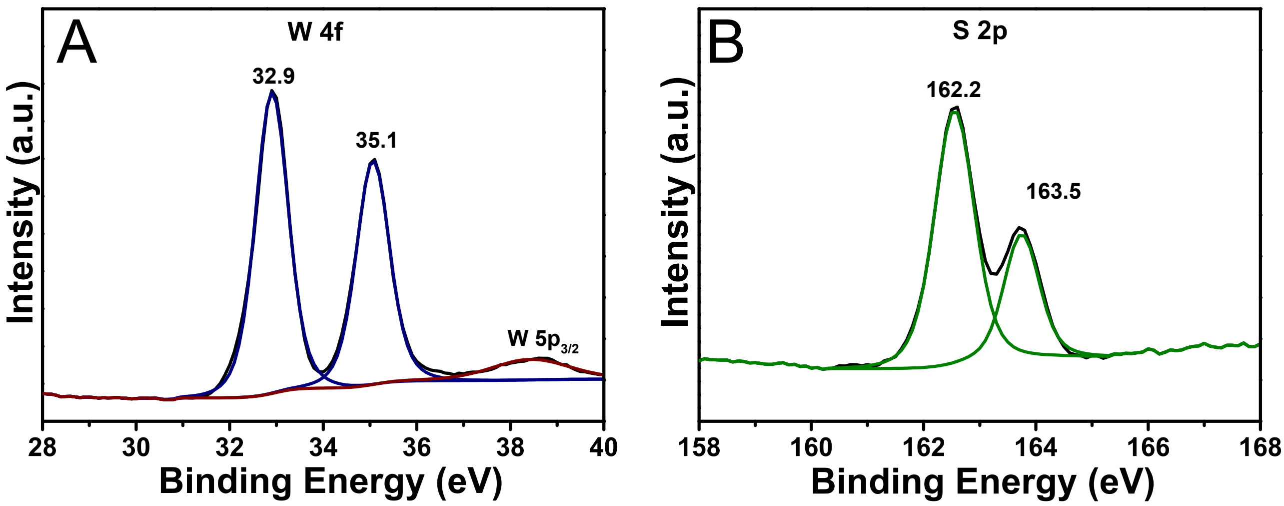

Figure S2: (A) W 4f (B) S2p XPS spectra obtained from CVD grown WS_2 domains. W 4f core level spectrum represents peaks at 32.9 eV, 35.1 eV and 38.5 eV those are corresponds to W $4f_{7/2}$, W $4f_{5/2}$ and W $5p_{3/2}$ states of tungsten. Sulfur S 2p peaks are observed at 162.2 eV and 163.5 eV, which are attributed to $S2p_{3/2}$ and $S2p_{1/2}$ respectively.

Section 1: Conductive AFM measurements

In the present case of nanoscale junctions, field induced tunneling may dominate over the TE component under reverse bias, especially for contact areas ~ 10 nm^2.[1,2] The intense junction electric field induced reduction in effective barrier width leads to large majority carrier (electron) injection from the metal to semiconductor CB, which is increasingly accentuated under increasing reverse bias.[1,2] Figures S3A and C schematically show the interfacial band bending illustrating the physics of tunnelling dominated reverse biased current exceeding the TE current under forward bias. In the reverse biased regime (V > 0 V) the IV curves are well described by the Fowler-Nordheim (FN) tunneling model,[3] which under forward bias (V < 0V) follows the TE model.[4] Figure S3B shows $ln\left(\frac{I}{V^2}\right)$ vs $\frac{1}{V}$ plots of the IV's shown in Figure 4E, in the V > 0 regime. The linearity of the plots in the large bias regime establishes validity of the FN tunneling model and the physical understanding presented above. The slope of the linear fits (black solid line in Figure S3B yields the local Schottky barrier parameter $(\boldsymbol{\alpha = \varphi_b^{3/2} d})$, where φ_b and d are the barrier height and width (see supplementary information for further details of the model parameters). We find $\boldsymbol{\alpha}$ varies between 2.32 – 2.17 for points 1 and 3 and reduces to 1.26 for point 2, which corresponds to the high current region around the core of the SDD spiral with high defect density and a higher electron density by consequence. Figure S3D shows the *ln(I) vs. V* plots corresponding to the different locations of spiral domain for V < 0 regime. The barrier height φ_b and ideality factor η were calculated from intercepts and slopes obtained from the linear fits in Figure S3D. The high values of η > 17 are suggestive of non-thermionic transport process even in the V < 0 regime, which are likely to be tunnelling of electrons from WS_2 to Au. φ_b shows a smaller relative variation with a value of 207 meV for the most conducting region (point 2), which increases to 280 meV for points 1 and 3.

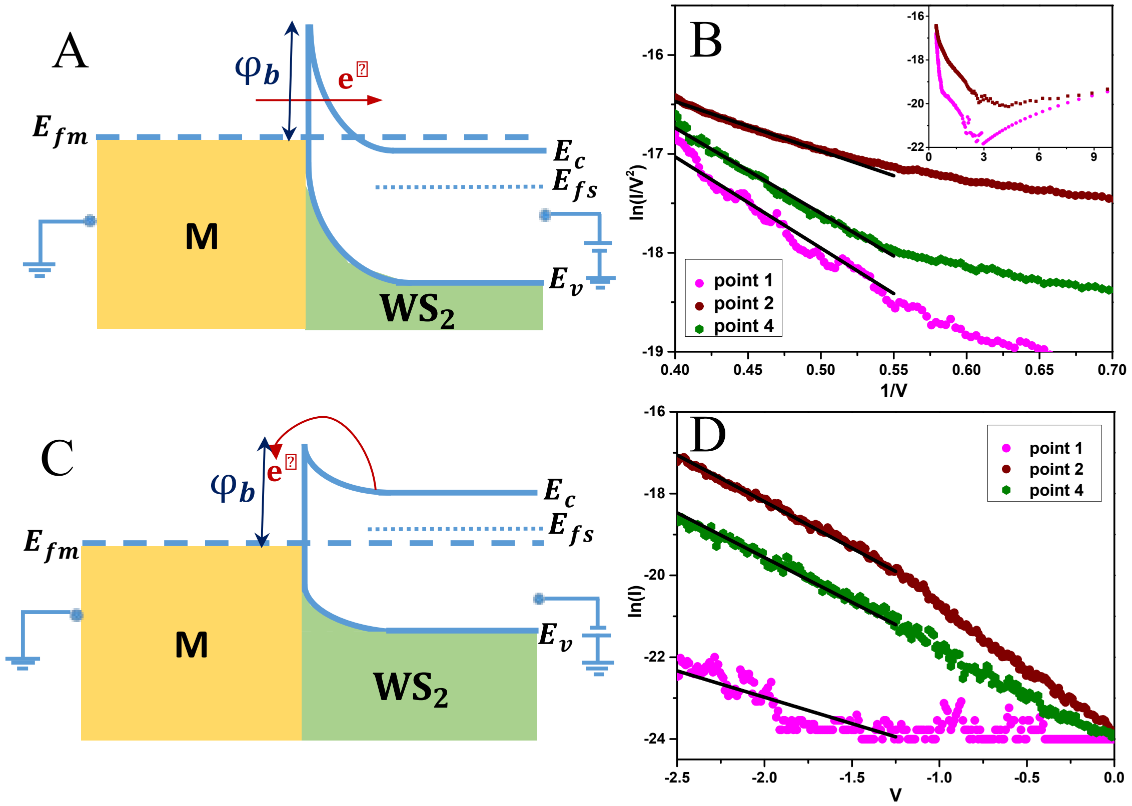

Figure S3: Schematic of M/S junction under (A) reverse bias & (C) forward bias (B) TE model & (D) FN tunnelling fit to experimental IV Curves for SDD spiral WS_2 domain.

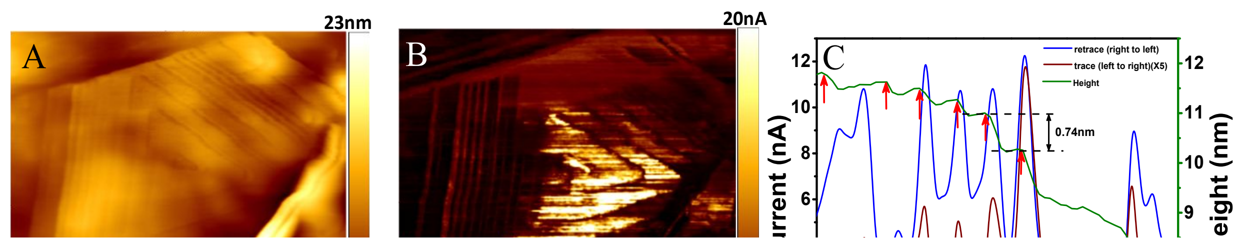

Figure S4: CVD grown spiral WS_2 AFM images: (A) topography (B) current map (C) line scan data of height, current (trace & retrace) showing WS_2 edges are more conducting compared to their plateau regions.

Figure S4A and B display height profile image and coreesponding current map of a spiral core structure respectively, which exhibiting a spiral layer thickness of ~ 0.74 nm. The correlated line scans across topography and current map sections are illustrated in Figure S4C. The current map shows that the edges of the spiral carry significantly more current than the plateau regions. The observation is further corroborated in the cross-sectional line scans which show a strong correlation between the position of the spiral edges in the topography and peaks in the local current (as indicated by red arrows in Figure S4C). The positional coincidence of the peaks in the current line scans obtained from trace and retrace current maps negate their origin from feedback related artifacts of the scan process.

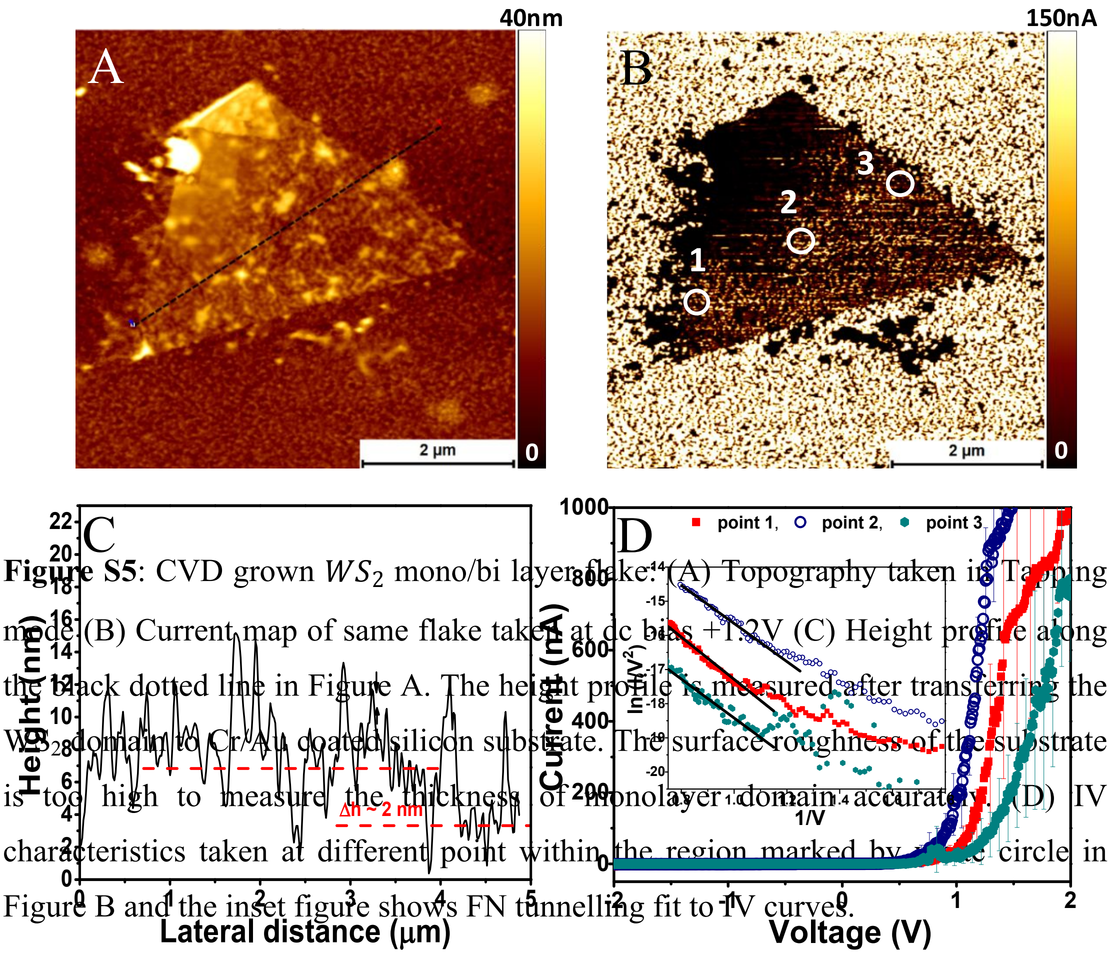

Figure S5: CVD grown WS_2 mono/bi layer flake: (A) Topography taken in Tapping mode (B) Current map of same flake taken at dc bias +1.2V (C) Height profile along the black dotted line in Figure A. The height profile is measured after transferring the WS_2 domain to Cr/Au coated silicon substrate. The surface roughness of the substrate is too high to measure the thickness of monolayer domain accurately. (D) IV characteristics taken at different point within the region marked by white circle in Figure B and the inset figure shows FN tunnelling fit to IV curves.

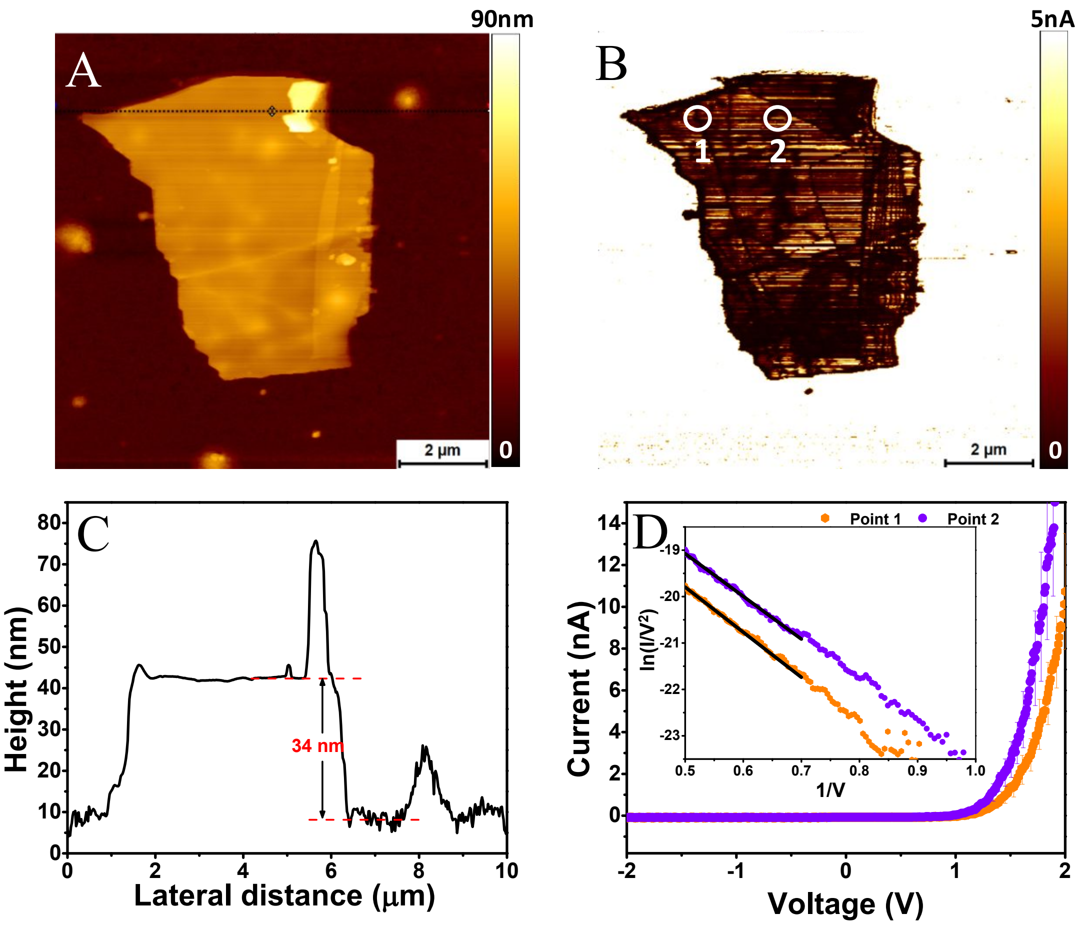

A
90nm
0
2 µm
B
5nA
1
2
0
2 µm
C
Height (nm)
34 nm
Lateral distance (µm)
D
Point 1
Point 2
Current (nA)
ln(I/V²)
1/V
Voltage (V)

Figure S6: Mechanically exfoliated WS_2 flake: (A) Topography (B) Current map taken at dc bias +1.2V (C) Height profile along the black dotted line in Figure A (D) IV characteristics taken at different point within the region marked by white circle in Figure B, inset shows FN tunnelling fit to IV curves.

FN analysis of local *IV* characteristics measured on the mono/bi-layer sample and the exfoliated one shows that Schottky barrier parameter ($\boldsymbol{\alpha}$) is lower for mono/bi-layer sample compared to the mechanically exfoliated sample (Figure S6) which reflects the enhanced effective conductivity of the thin CVD sample compared to the exfoliated one.

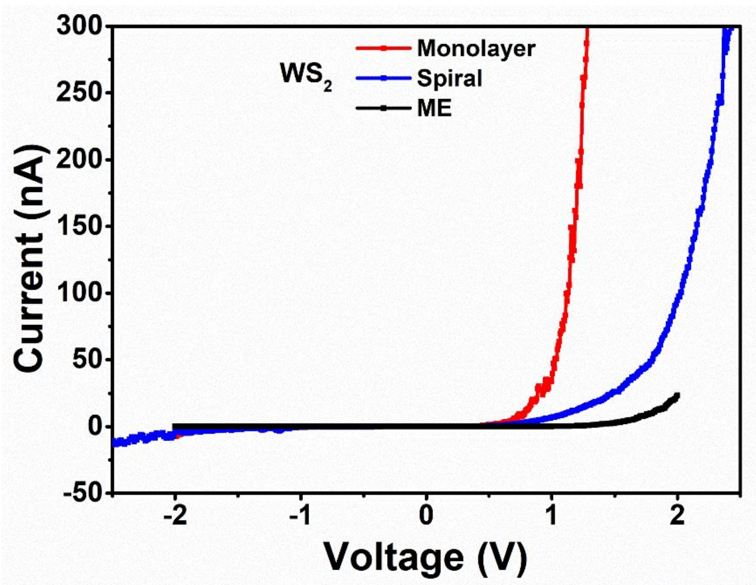

Figure S7: Comparing conducting AFM vertical I-V response from WS_2 spiral, monolayer and mechanically exfoliated flakes.

Section 2: Electrocatalytic microcell fabrication

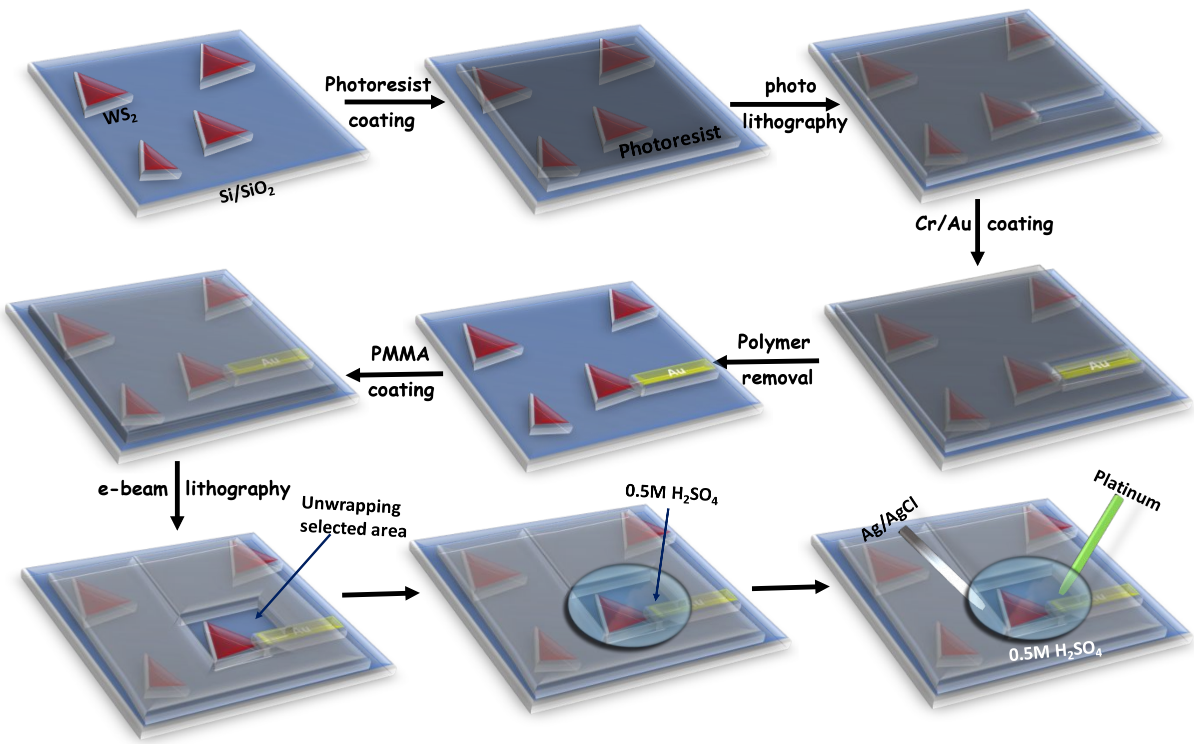

Figure S8: Schematic illustrating various steps involved in μ-electrochemical device fabrication

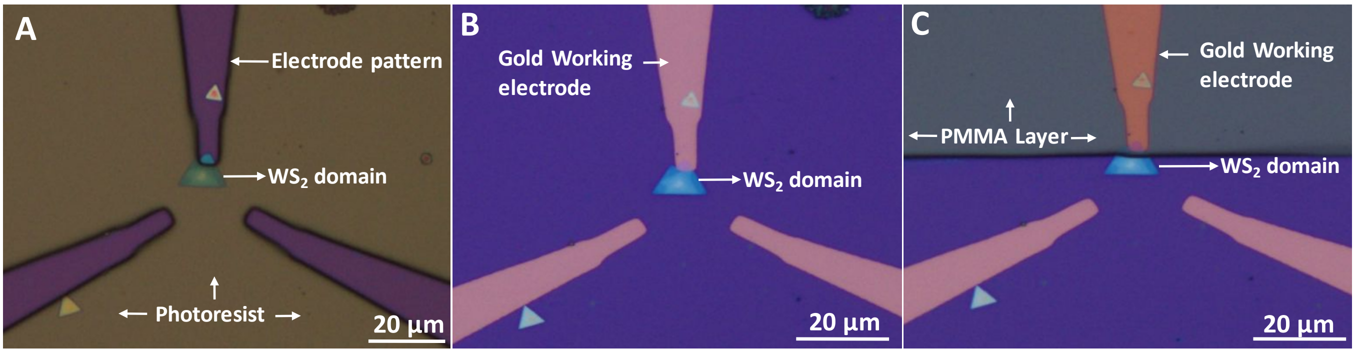

Figure S9: Optical images of WS_2 domain during different lithography steps. (A) Image of WS_2 sample after photopolymer coating and photolithography. (B) Image after electrode deposition and photopolymer removal. (C) After PMMA coating and e-beam lithography step.

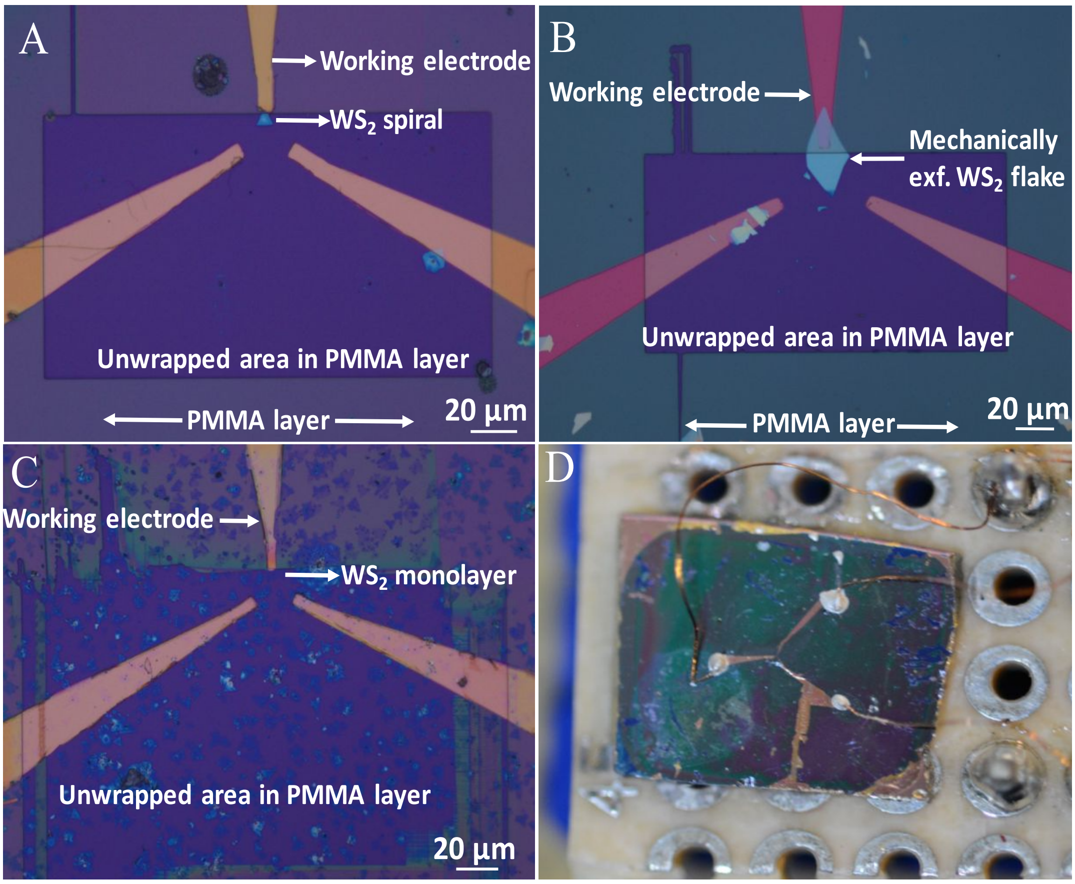

Figure S10: Various devices fabricated in the current study. (A) Spiral WS_2 (B) mechanically exfoliated WS_2 and (C) Monolayer domain. (D) Photograph of the fabricated microcell device.

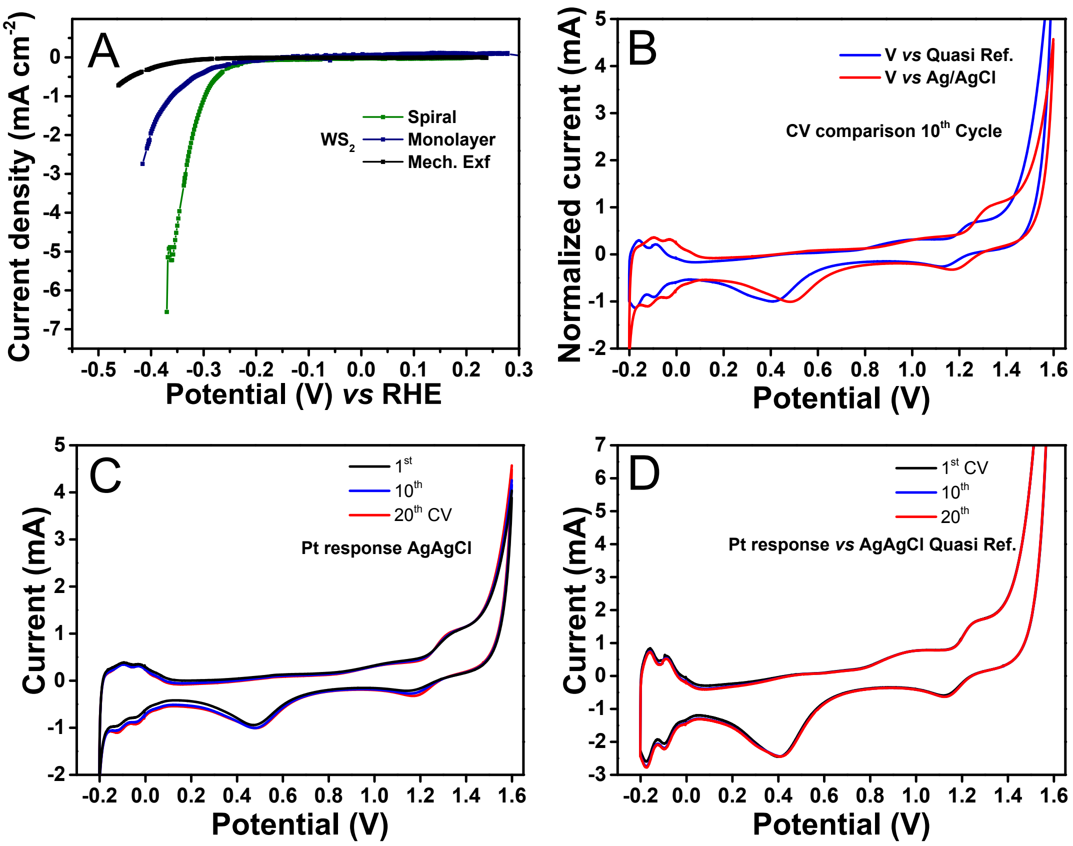

Figure S11: (A) Polarization curve replotted *w.r.t* RHE. (B) Platinum response comparison in acidic media using Ag/AgCl reference and AgCl coated Ag wire quasi-reference electrode after 10^{th} cycle. Platinum response in acidic media using (C) Ag/AgCl reference and (D) AgCl coated Ag wire quasi-reference electrode.

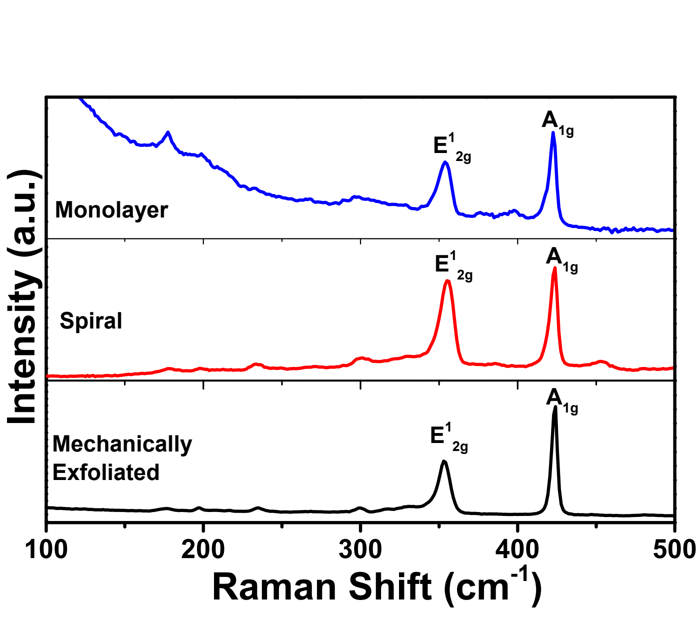

Figure S12: Raman spectra of WS_2 domains after HER measurements collected using 632 nm laser excitation.

Table S1: Comparison of various TMD single domain HER measurements

No.	Catalyst	HER comparison (*vs* RHE)	Reference
1	2H MoS_2	4 mA cm^{-2} @ 600 mV	Nat. Commun. 2016, 7, 11857[5]
2	1T MoS_2 2H MoS_2	607 mA cm^{-2} @ 400 mV 43 mA cm^{-2} @ 400 mV	Nat. Chem. 2018, 10, 638-643[6]
3	2H MoS_2 1T MoS_2	10 mA cm^{-2} @ 420 mV 10 mA cm^{-2} @ 300 mV	Adv. Mater. 2017, 29, 1701955[7]
4	2H MoS_2 edge exposed	10-50 mA cm^{-2} @ 400 mV	Nat. Mater. 2016, 15, 1003-1009[8]
5	WS_2 spirals	5 mA cm^{-2} @ 347 mV	Current work

REFERENCES

1. Rezeq, M. d.; Ali, A.; Patole, S. P.; Eledlebi, K.; Dey, R. K.; Cui, B., The Dependence of Schottky Junction (I–V) Characteristics on the Metal Probe Size in Nano Metal–Semiconductor Contacts. *AIP Adv.* **2018,** *8*, 055122.

2. Son, Y.; Wang, Q. H.; Paulson, J. A.; Shih, C.-J.; Rajan, A. G.; Tvrdy, K.; Kim, S.; Alfeeli, B.; Braatz, R. D.; Strano, M. S., Layer Number Dependence of MoS_2 Photoconductivity Using Photocurrent Spectral Atomic Force Microscopic Imaging. *ACS Nano* **2015,** *9*, 2843-2855.
3. Fowler Ralph, H.; Nordheim, L., Electron Emission in Intense Electric Fields. *P. ROY. SOC. A -MATH. PHY.* **1928,** *119*, 173-181.
4. Sze, S. M.; K. Ng, K., *Physics of Semiconductor Devices*. Third ed.; Wiley-Interscience: 2006.
5. Cummins, D. R.; Martinez, U.; Sherehiy, A.; Kappera, R.; Martinez-Garcia, A.; Schulze, R. K.; Jasinski, J.; Zhang, J.; Gupta, R. K.; Lou, J.; Chhowalla, M.; Sumanasekera, G.; Mohite, A. D.; Sunkara, M. K.; Gupta, G., Efficient Hydrogen Evolution in Transition Metal Dichalcogenides *via* A Simple One-Step Hydrazine Reaction. *Nat. Commun.* **2016,** *7*, 11857.
6. Yu, Y.; Nam, G.-H.; He, Q.; Wu, X.-J.; Zhang, K.; Yang, Z.; Chen, J.; Ma, Q.; Zhao, M.; Liu, Z.; Ran, F.-R.; Wang, X.; Li, H.; Huang, X.; Li, B.; Xiong, Q.; Zhang, Q.; Liu, Z.; Gu, L.; Du, Y.; Huang, W.; Zhang, H., High Phase-Purity 1T′-MoS_2- and 1T′-$MoSe_2$-Layered Crystals. *Nat. Chem.* **2018,** *10*, 638-643.
7. Zhang, J.; Wu, J.; Guo, H.; Chen, W.; Yuan, J.; Martinez, U.; Gupta, G.; Mohite, A.; Ajayan, P. M.; Lou, J., Unveiling Active Sites for the Hydrogen Evolution Reaction on Monolayer MoS_2. *Adv. Mater.* **2017,** *29*, 1701955.
8. Voiry, D.; Fullon, R.; Yang, J.; de Carvalho Castro e Silva, C.; Kappera, R.; Bozkurt, I.; Kaplan, D.; Lagos, M. J.; Batson, P. E.; Gupta, G.; Mohite, Aditya D.; Dong, L.; Er, D.; Shenoy, V. B.; Asefa, T.; Chhowalla, M., The Role of Electronic Coupling Between Substrate and 2D MoS_2 Nanosheets in Electrocatalytic Production of Hydrogen. *Nat. Mater.* **2016,** *15*, 1003.